Co-Estimation of State-of-Charge and State-of-Health for Lithium-Ion Batteries Considering Temperature and Ageing

Xin Lai [1], Ming Yuan [1], Xiaopeng Tang [2,*], Yi Yao [1], Jiahui Weng [1], Furong Gao [2], Weiguo Ma [3] and Yuejiu Zheng [1]

[1]   School of Mechanical Engineering, University of Shanghai for Science and Technology, Shanghai 200093, China
[2]   Department of Chemical and Biological Engineering, Hong Kong University of Science and Technology, Hong Kong, China
[3]   School of Electrical Engineering, Nantong University, Nantong 226019, China
*   Correspondence: xtangai@connect.ust.hk

Abstract: State-of-charge (SOC) estimation of lithium-ion batteries (LIBs) is the basis of other state estimations. However, its accuracy can be affected by many factors, such as temperature and ageing. To handle this bottleneck issue, we here propose a joint SOC-SOH estimation method considering the influence of the temperature. It combines the Forgetting Factor Recursive Least Squares (FFRLS) algorithm, Total Least Squares (TLS) algorithm, and Unscented Kalman Filter (UKF) algorithm. First, the FFRLS algorithm is used to identify and update the parameters of the equivalent circuit model in real time under different battery ageing degrees. Then, the TLS algorithm is used to estimate the battery SOH to improve the prior estimation accuracy of SOC. Next, the SOC is calculated by the UKF algorithm, and finally, a more accurate SOH can be obtained according to the UKF-based SOC trajectory. The battery-in-the-loop experiments are utilized to verify the proposed algorithm. For the cases of temperature change up to 35 °C and capacity decay up to 10%, our joint estimator can achieve ultra-low errors, bounded by 2%, respectively, for SOH and SOC. The proposed method paves the way for the advancement of battery use in applications, such as electric vehicles and microgrid applications.

Keywords: lithium-ion batteries; joint SOC-SOH estimation; forgetting factor recursive least squares; total least squares; unscented Kalman filter

1. Introduction

Energy crises and environmental pollution are the main obstacles restricting the sustainable development of the economy and society. In this context, electric vehicles (EVs) have developed rapidly worldwide because of their advantages in environmental protection and energy conservation [1–5]. As the core component of EVs, lithium-ion batteries (LIBs) have significant benefits, such as long cycle life, high energy density, and low self-discharge rate [6–11]. Since Li-ion batteries are easily affected by usage conditions and environments, a battery management system (BMS) is essential in ensuring battery safety and reliability. State estimation of LIBs is one of the core functions of BMS. Common states include state-of-charge (SOC), state-of-health (SOH), state-of-energy (SOE), state-of-power (SOP), etc. [12–14]. SOC and SOH are, respectively, the indicators for remaining driving distance and ageing degree [15–17]. However, due to the unaffordable cost of integrating sensors into the batteries [18], these implicit states cannot be directly measured by commercial BMSs. As a response, state estimation techniques, which indirectly calculate the internal states of the batteries from available signals such as current, voltage, and temperature, are gaining popularity.

SOC represents the ratio of the remaining capacity of LIB to its full charge capacity, whose estimation is the basis of the other state observers. However, as revealed by [19], the

accuracy of the SoC calculator is affected by factors such as battery ageing, ambient temperature, and sensor noise. Therefore, conventional approaches, such as the ampere-hour integral method and standard OCV method, are less effective in this kind of complicated usage scenario. Compared with these simple algorithms, model-based approaches exhibit better adaptiveness to these factors and have become the mainstream for online SOC estimation [20]. Commonly used models can be categorized into three types, namely, first-principle models, electric circuit models, and data-driven models.

First-principle models refer to models that describe the process of chemical changes in batteries. Pseudo Two-Dimensional (P2D) model and Single Particle (SP) model [21–24] are the most representative examples. Though theoretically accurate, they require a deep understanding of electrochemical natures, which may vary with battery materials [17,25]. In addition, these models are usually complicated to implement due to the involvement of partial differential equations [26]. Therefore, they are more suitable for theoretical analysis and less effective for onboard applications.

Data-driven models, as the name implies, rely purely on the data. Commonly seen examples include neural networks (NN) [27], support vector regression (SVR) [28], Gaussian process regression (GPR) [29], and extreme learning machine (ELM) [30,31]. Without using any prior knowledge of the chemistry nature, data-driven models can be used to describe all types of LIBs. However, as a common issue for these data-driven methods, these models require a large amount of data for training to improve accuracy, and their generalization to untrained cases is usually weak. Since the real-life battery using profiles contain high uncertainties, considerable training data should be used to ensure estimation accuracy in different scenarios.

Compared with the above two model types, ECM, which uses RC networks to simulate battery dynamics, offers a good balance between complexity and accuracy. As a result, various methods are combined with the ECMs to implement SOC estimation. Commonly used algorithms include Kalman Filters [32–34], Particle Filters [35], and some light-weighted approaches such as Luenberger observer [36], PI observer [37], sliding mode observer [38], and local least squares [39].

It is worth pointing out that the accuracy of these algorithms relies on not only the quality of the filtering methods but also the modeling accuracy. As is the case with most electrochemical systems, the model parameters of LIBs will change gradually with battery ageing and temperature, and the resulted model mismatch will lead to large SOC estimation errors [40]. Understanding that the SOH estimation also relies on an accurate SOC estimation, joint state estimation frameworks for SOC and SOH have been developed to handle this kind of circular dependence. Specifically, Yu et al. [40] used the Recursive Least Square (RLS) algorithm to realize the online parameter identification of ECM and then combined it with the adaptive H∞ filter to estimate battery SOH. Tan et al. [41] proposed an EKF-RLS-based dynamic parameter identification algorithm with a multi-timescale and conducted an online SOH estimation based on the SVR algorithm. Yan et al. [42] estimated the battery SOH and predicted the remaining service life based on Lebesgue sampling. Tang et al. [43] used V-min EKF to estimate the SOC and explored a balancing current ratio technique to estimate the SOH for all cells in a battery pack.

Though effective, it is worth pointing out that most joint SOC-SOH estimation frameworks do not consider the influence of temperature on model parameters. In addition, they do not use an estimated state (e.g., SOH) to improve the accuracy of the other estimates (e.g., SOC), leaving space to improve the overall accuracy. Aiming at these issues, we here propose a joint SOC-SOH estimation method. Specifically, the FFRLS algorithm is first used to identify the parameters of ECM in the battery ageing process online, and the battery model is then updated in real-time. Next, the battery capacity and SOH are calculated by using the TLS algorithm with the identified parameters. Based on the updated model parameters and capacity, the SOC is estimated using the UKF algorithm. Finally, the battery SOH is calculated again using the TLS algorithm and the estimated SOC trajectories. The effectiveness of our "two-stage" estimation strategy is verified with the battery-in-the-loop

experiments. The main potential contributions of this work can be summarized as follows: (1) A new joint SOC-SOH estimation framework is proposed. In particular, a "two-stage" estimation strategy is proposed to improve SOH estimation accuracy. (2) SOC and SOH are accurately co-estimated online with a low computational cost against temperature change and battery ageing.

The remainder of this paper is organized as follows: Battery modeling is described in Section 2. The method of joint SOC-SOH estimation is described in Section 3. The results and conclusions are given in Sections 4 and 5, respectively.

2. Battery Modeling

2.1. Equivalent Circuit Model

ECM balances model accuracy and complexity and is widely used in battery state estimation [44,45]. The RC elements in the ECM can simulate the chemical diffusion and polarization process inside the battery, and it is divided into 1RC, 2RC, 3RC, and n-RC models. In this study, the 1RC model is used because it provides a good balance between model robustness and complexity [46]. Its structure is shown in Figure 1.
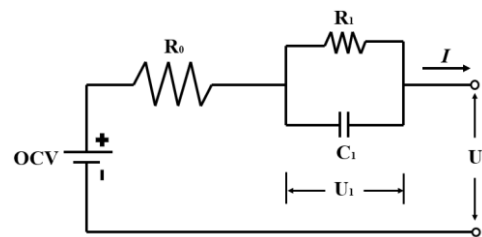

Figure 1. 1RC model.

The mathematical expression of the 1RC model is as follows:

$$U_k = OCV(SOC_k) - I_k \cdot R_0 - U_{1,k} \tag{1}$$

$$U_{1,k+1} = U_{1,k} \cdot exp(-t/\tau_1) + I_k \cdot R_1 \cdot [1 - exp(-t/\tau_1)] \tag{2}$$

$$\tau_1 = R_1 \cdot C_1 \tag{3}$$

where subscript k is the time k, U_t is the battery terminal voltage, U_1 is the polarization voltage, I is the working current (positive when charging the battery), R_0 is ohmic resistance, R_1 is polarization resistance, C_1 is polarization capacitance, τ_1 is time constant, t is the time, $OCV()$ is a nonlinear function describing the relationship between the battery's OCV and SOC, and SOC is the battery's state-of-charge, also defined as the remaining percentage of the battery's available capacity.

Recall the transfer function of the RC series circuit in the frequency domain:

$$H_a(s) = \frac{1}{\tau \cdot s + 1} \tag{4}$$

where s is a complex variable in the Laplace transform.

By using bilinear transformation to discretize Equation (4), we get:

$$H_d = H_a\left(\frac{2}{\Delta T} \cdot \frac{z-1}{z+1}\right) = \frac{1}{(1 + \frac{2}{\Delta T} \cdot R_1 C_1) + (1 - \frac{2}{\Delta T} \cdot R_1 C_1) \cdot z^{-1}} \tag{5}$$

where ΔT is the sampling interval, z is a complex variable in the Z-transformation.

According to the 1RC equivalent circuit structure, the converted transfer function is:

$$G(z) = \frac{U_t(z) - OCV(z)}{I_z} = -[R_0 + R_1 \cdot H_d(z)] \tag{6}$$

Substituting Equation (5) into Equation (6) yields the transfer function as:

$$G(z) = -\frac{\frac{(R_0+R_1)\Delta T+2R_0R_1C_1}{\Delta T+2R_1C_1} + \frac{(R_0R_1)\Delta T-2R_0R_1C_1}{\Delta T+2R_1C_1} \cdot z^{-1}}{1 + \frac{\Delta T-2R_1C_1}{\Delta T+2R_1C_1} \cdot z^{-1}} \tag{7}$$

Equation (7) can be further simplified as follows:

$$G(z) = \frac{U_t(z) - OCV(z)}{I(z)} = \frac{a_2 + a_3 \cdot z^{-1}}{1 + a_1 \cdot z^{-1}} \tag{8}$$

which can be given as follows:

$$a_1 = -\frac{\Delta T - 2R_1C_1}{\Delta T + 2R_1C_1} \tag{9}$$

$$a_2 = -\frac{(R_0 + R_1)\Delta T + 2R_0R_1C_1}{\Delta T + 2R_1C_1} \tag{10}$$

$$a_3 = -\frac{(R_0 + R_1)\Delta T - 2R_0R_1C_1}{\Delta T + 2R_1C_1} \tag{11}$$

Or equivalently:

$$R_0 = \frac{a_3 - a_2}{1 + a_1} \tag{12}$$

$$R_1 = -\frac{a_3 + a_2}{1 - a_1} - R_0 \tag{13}$$

$$\tau_1 = R_1C_1 = \frac{\Delta T}{2} \cdot \frac{1 + a_1}{1 - a_1} \tag{14}$$

By converting Equation (8) back to the (discretized) time domain and assuming that the battery's OCV tends to be stable in a short period (say, OCV_k approximately equals to OCV_{k-1}), we have:

$$U_{t,k} = a_1 U_{t,k-1} + (1 - a_1)OCV_k + a_2 I_k + a_3 I_{k-1} \tag{15}$$

Equation (15) can be re-written as:

$$y_k = U_{t,k} = \varphi_k^T \cdot \theta_k \tag{16}$$

with $\varphi_k = [1, U_{t,k-1}, I_k, I_{k-1}]^T$ and $\theta_k = [(1 - a_1)OCV_k, a_1, a_2, a_3]^T$.

It is worth pointing out that our modeling strategy is different from those in Ref [47], as OCV is also treated as a parameter to be identified in Equation (16). In this way, we can use the identified OCV to implement the calculation of battery SOH while avoiding the "circular dependence" issue (see Section 3.1 for details).

2.2. Online Parameter Identification

To ensure the modeling accuracy under various battery temperatures and ageing degrees, we need to update the model parameters in real time. At present, model identification algorithms, such as the PSO and GA, are widely adopted [48]. However, these algorithms suffer from high computational costs and are, therefore, not suitable for online applications. The least square method is simple and requires no prior statistics. It is widely used for online parameter identification [49]. However, a converged least square algorithm is less sensitive to the new data [50], resulting in a gradual increase in error. To address this issue, we here introduce the FFRLS algorithm to identify the model parameters online. The process of online identification by the FFRLS algorithm is shown in Figure 2. The specific process is as follows:

(1) System input vector:

$$y_{k+1} = \varphi_{k+1}^T \hat{\theta}_{k+1} \tag{17}$$

(2) Estimated error:

$$e_{k+1} = y_{k+1} - \varphi_{k+1}^T \hat{\theta}_k \tag{18}$$

(3) Gain vector:

$$K_{k+1} = P_k \varphi_{k+1} (\lambda + \varphi_{k+1}^T P_k \varphi_{k+1})^{-1} \tag{19}$$

(4) Parameter vector to be evaluated:

$$\hat{\theta}_{k+1} = \hat{\theta}_k + K_{k+1} e_{k+1} \tag{20}$$

(5) Update covariance matrix:

$$P_{k+1} = \frac{1}{\lambda} (I - K_{k+1} \varphi_{k+1}^T) P_k \tag{21}$$

where $\hat{\theta}$ is the estimated parameter vector in Equation (17), e is estimation error, K is the gain matrix, P is the covariance matrix, I is the identity matrix, and λ is the forgetting factor, which is added to the conventional RLS algorithm to reduce the weight of old data and improve the accuracy of online parameter identification under dynamic conditions.
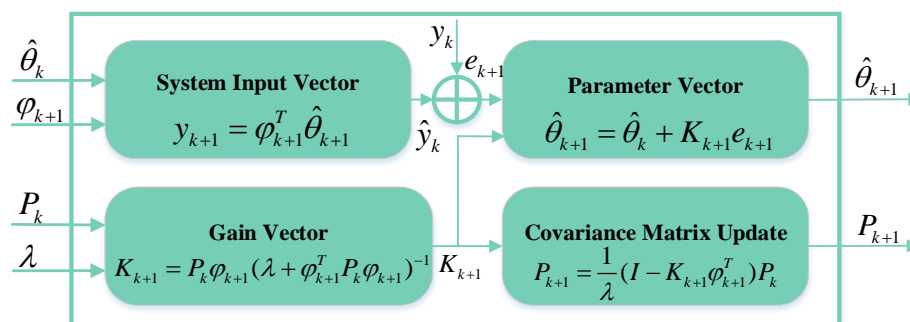

Figure 2. The parameter identification process of the FFRLS algorithm.

When using the FFRLS algorithm, initial parameters (a_1, a_2 and a_3) are calculated by interpolating the data obtained from the parameter identification of fresh battery. Then, the vector θ_k is determined, and the measurement vector φ_k and input vector y_k are determined according to the measured current and voltage data. Afterwards, the estimated error e_k is calculated. The gain vector K_k is calculated based on the covariance matrix P_k, measurement vector φ_k, and forgetting factor λ. Finally, the estimated parameter vector θ_k is calculated, and the model parameters can then be updated according to Equations (9)–(14). It should be noted that the measured battery voltage and current change with the battery ageing and temperature. In this case, the model parameters identified in real-time by the FFRLS algorithm will change to minimize the model and measured voltages. Therefore, the proposed algorithm can realize the real-time online identification and update of battery model parameters and OCV under complex conditions.

3. Joint SOC-SOH Estimation Method

3.1. SOH Estimation

The battery's SOH is not only an important indicator of the ageing status but also a key prior knowledge for accurate SOC estimation. We do have multiple algorithms to obtain battery SOH, such as using ICA-based calculous [51]. However, when an accurate SOC trajectory is available, the most used battery capacity estimation method is the "Two-

Point" [52]. This method calculates the battery's current capacity based on the change in charge and SOC between the time interval $t_1 \rightarrow t_2$, which can be described as follows:

$$SOH = \left. \frac{\int_{t_1}^{t_2} \frac{\eta I(t)}{3600} dt}{SOC(t_2) - SOC(t_1)} \right/ Cap_0 \qquad (22)$$

where $SOC(t_1)$ and $SOC(t_2)$ are the corresponding battery SOC at two different times, t_1 and t_2, respectively, Cap_0 is the battery's initial capacity, and η is Coulomb efficiency, which is commonly treated as 1.

In this work, our SOH estimation contains two stages. In the first stage, a SOH value is calculated following the idea of Equation (22), where the SOC is obtained by feeding the OCV identified from Equations (17)–(21) into a static OCV-SOC lookup table. Though less accurate, this SOH can be used to compensate for the large capacity deviation of the aged batteries to facilitate the follow-up SOC calculation. In the second stage, the SOH is calculated again following the idea of Equation (22), but the SOC is obtained from the powerful UKF algorithm (see Section 3.2 for details) to improve its accuracy. Noting that two different models are utilized to obtain the SOC, our two-stage SOH estimator will not suffer from the issue of "circular dependence". In this work, our OCV-SOC trajectory is obtained through the Hybrid Pulse Power Characteristic (HPPC) test at 25 °C, a detailed experimental procedure that can be found in our previous work [53]. For clarity, the identified OCV-SOC curve of our battery is shown in Figure 3.
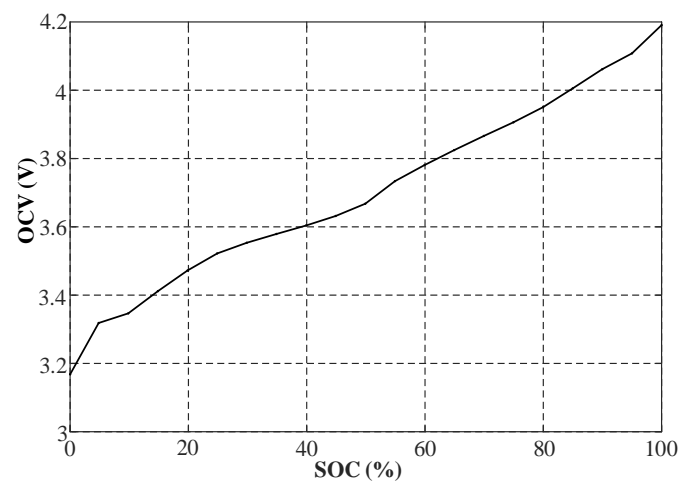
Figure 3. OCV-SOC curve.

Noting that the "Two-Point" method suffers from the local perturbance in SOC estimation, rather than directly using Equation (22), the total least square (TLS) algorithm [54] is used to estimate the capacity online. Re-write Equation (22) as:

$$SOC(t_2) - SOC(t_1) = \frac{1}{Cap_0} \int_{t_1}^{t_2} \frac{\eta I(t)}{3600} dt \qquad (23)$$

Marking $x_i = \int_{t_1}^{t_2} \frac{\eta I(t)}{3600} dt$, and $y_i = SOC(t_2) - SOC(t_1)$, the following expression can be obtained:

$$y_i = \beta_1 + \beta_2 x_i + v_i \qquad (24)$$

where β_1 is an estimated constant, β_2 is an estimated coefficient with $Cap = 1/\beta_2$ and v_i is the noise in the estimation process.

By accumulating data from time m to time n ($1 < m < n$), Equation (24) can be expressed in vector form as:

$$
\begin{bmatrix} y_m \\ y_{m+1} \\ \vdots \\ y_n \end{bmatrix} = \begin{bmatrix} 1 & x_{m,1} \\ 1 & x_{m+1,1} \\ \vdots & \vdots \\ 1 & x_{n,1} \end{bmatrix} \begin{bmatrix} \beta_1 \\ \beta_2 \end{bmatrix} + \begin{bmatrix} v_m \\ v_{m+1} \\ \vdots \\ v_n \end{bmatrix}
\tag{25}
$$

Then, Equation (25) can be converted into matrix form:

$$
Y = X \cdot H + V
\tag{26}
$$

where Y is the observation vector, X is a known matrix, $H = [\beta_1, \beta_2]^T$ is the parameter vector, and V is the random error vector.

The parameter vector H can be solved by the analytic expression of the TLS algorithm:

$$
H = (X^T X - \sigma_{n+1}^2 E)^{-1} X^T Y
\tag{27}
$$

where σ_{n+1} is the smallest singular value of $[X\ Y]$, E is the identity matrix. Then, the TLS-based capacity can be estimated by:

$$
Cap_{TLS} = 1/H(2)
\tag{28}
$$

Dividing the estimated capacity by the fresh-cell-capacity, we obtain the estimated SOH:

$$
SOH = \frac{Cap_{TLS}}{Cap_0}
\tag{29}
$$

The above process is utilized for both the first-stage and the second-stage SOH estimation. The only difference here is the method of acquiring battery SOC.

3.2. SOC Estimation

3.2.1. UKF Algorithm

Kalman Filter (KF) algorithm is widely used as the state observer, and the EKF algorithm, which uses Tayer expansion to provide first-order model linearization, is the most commonly used for SOC estimation in BMS [55]. However, batteries are highly nonlinear systems, and using only first-order approximation will significantly influence the estimation accuracy. Therefore, the UKF algorithm [56,57] is employed to estimate SOC in this study. UKF algorithm deals with nonlinear systems by using the idea of the probability distribution, which approximately replaces the linearization of the propagation mode of statistical characteristics in EKF with an unscented transform (UT). UT will not directly omit the higher-order terms but obtain some sampling points near the estimation points according to certain calculation rules and use these sampling points to approximate the probability density function of the state [58]. In general, UT could achieve 3-order approximating accuracy for Gaussian inputs and at least 2-order accuracy for non-Gaussian cases. The specific implementation process is as follows:

(1)   Obtaining the $2n + 1$ Sigma points:

$$
\begin{cases}
Z_0 = \overline{Z}, i = 0 \\
Z_i = \overline{Z} + (\sqrt{(n + \lambda)P})_i, i = 1, \ldots, n \\
Z_i = \overline{Z} - (\sqrt{(n + \lambda)P})_i, i = n + 1, \ldots, 2n
\end{cases}
\tag{30}
$$

where Z is the sampling point after UT, $\overline{Z}$ is the mean value of random variables, n is the dimension of the state vector, and P is the error covariance matrix.

(2) Weighting of each Sigma point:

$$\begin{cases} \omega_m^{(0)} = \frac{\lambda}{n+\lambda} \\ \omega_c^{(0)} = \frac{\lambda}{n+\lambda} + (1-\alpha^2+\beta) \\ \omega_m^{(i)} = \omega_c^{(i)} = \frac{\lambda}{2(n+\lambda)}, i=1,\dots,2n \end{cases} \tag{31}$$

where $\lambda = \alpha^2(n+\kappa) - n$ is the adjustment parameter, α denotes the distance from the sampling point to the mean point, which is usually set to a small positive number, κ is usually taken as 0 or 3, and β describes the distribution information.

After UT, the statistical characteristics of the new sampling points are used to describe the nonlinear equation, which avoids the error caused by directly ignoring the high-order terms and effectively improves the filter accuracy.

3.2.2. SOC Estimation Based on UKF Algorithm

To implement the UKF algorithm, we first discrete the battery model, with the results given in Equations (32)–(34). Here Δt is the sampling interval, R_0 is ohmic resistance, R_1 is polarization resistance, τ_1 is time constant, I_k is working current, η is Coulomb efficiency, Cap_{TLS} is the current capacity estimated online by the TLS algorithm, w_k is state transition noise, and v_k is measurement noise.

$$SOC_{k+1} = SOC_k + \frac{\eta I_k}{3600 Cap_{TLS}} + w_{1,k} \tag{32}$$

$$U_{1,k+1} = U_{1,k}\exp\left(-\frac{\Delta t}{\tau_1}\right) - R_1\left(1 - \exp\left(-\frac{\Delta t}{\tau_1}\right)\right) \cdot I_k + w_{2,k} \tag{33}$$

$$U_{t,k} = OCV(SOC_k) - I_k R_0 - U_{1,k} + v_k \tag{34}$$

Then, the current is treated as the system's input, and SOC and polarization voltage are regarded as state variables and estimated simultaneously from the measured voltage. The state vectors SOC and $U_{1,k}$ can also be written in the form of vectors, which is shown in Equation (35). The system observation value y_k is the battery's terminal voltage $U_{t,k}$, as shown in Equation (36), and the working current I_k is treated as the system excitation, as shown in Equation (37).

$$x_k = \begin{bmatrix} SOC_k \\ U_{1,k} \end{bmatrix} \tag{35}$$

$$y_k = U_{t,k} \tag{36}$$

$$u_k = I_k \tag{37}$$

With these definitions, Equations (35) and (37) can be re-written as

$$x_{k+1} = Ax_k + Bu_k + Q \tag{38}$$

with $A = \begin{bmatrix} 1 & 0 \\ 0 & \exp(-\frac{\Delta t}{\tau_1}) \end{bmatrix}$, $B = \begin{bmatrix} \frac{\eta}{3600 \cdot Cap_{TLS}} \\ -R_1 \cdot (1 - \exp(-\frac{\Delta t}{\tau_1})) \end{bmatrix}$, and $Q = \begin{bmatrix} w_{1,k} \\ w_{2,k} \end{bmatrix}$.

The state equation and observation equation of a nonlinear system can be expressed in Equations (39) and (40):

$$x_{k+1} = f(x_k, u_k) + w_k \tag{39}$$

$$y_k = g(x_k, u_k) + v_k \tag{40}$$

According to UT, state transition equation, and observation equation, the calculation process of the UKF algorithm is listed in Algorithm 1.

Algorithm 1. The calculation process of the UKF algorithm.

---

(1) Initialization parameters:The error covariance matrix P, usually taken as $P = 10^{-6} * \begin{bmatrix} 1 & 0 \\ 0 & 1 \end{bmatrix}$.

---

(2) Iterative calculation, $k = 1, 2, \dots, N$:

(a) The state vector is transformed by the UT, and the Sigma points of the state vector x_k and the weight of each Sigma point are calculated according to Equations (30) and (31).

(b) State transfer of Sigma points:

$$x_k^{(i),-} = f(x_{k-1}^{(i),-}, u_{k-1}) + w_{k-1} \tag{41}$$

(c) Calculating the updated state vector x_k^- and error covariance matrix P_k^- according to Sigma points and weight:

$$x_k^- = \sum_{i=0}^{2n} \omega_m^{(i)} x_k^{(i),-} \tag{42}$$

$$P_k^- = \sum_{i=0}^{2n} \omega_c^{(i)} [x_k^- - x_k^{(i),-}][x_k^- - x_k^{(i),-}]^T + Q \tag{43}$$

(d) The predicted value of the state vector is transformed by UT, and the new Sigma points and the weight of each Sigma point are calculated.

(e) The new Sigma points are brought into the observation Equation (40), and the observation values are obtained:

$$y_k^{(i)} = g(x_k^{(i),-}, u_k) + v_k \tag{44}$$

(f) The mean value of the observed value y_k, error covariance $P_{y_k y_k}$, and $P_{x_k y_k}$ are obtained by weighted calculation:

$$y_k = \sum_{i=0}^{2n} \omega_m^{(i)} y_k^{(i)} \tag{45}$$

$$P_{y_k y_k} = \sum_{i=0}^{2n} \omega_c^{(i)} [y_k^{(i)} - y_k][y_k^{(i)} - y_k] + R \tag{46}$$

$$P_{x_k y_k} = \sum_{i=0}^{2n} \omega_c^{(i)} [x_k^{(i),-} - x_k^-][y_k^{(i)} - y_k] \tag{47}$$

where R is measurement noise, and $R = 10^{-3}$.

(g) Calculating the Kalman gain K_k:

$$K_k = P_{y_k y_k}^{-1} P_{x_k y_k} \tag{48}$$

(h) Updating the state vector x_k^+ and covariance matrix P_k:

$$x_k^+ = x_k^- + K_k(U_{t,k} - y_k) \tag{49}$$

$$P_k = P_k^- - K_k P_{y_k y_k} K_k^T \tag{50}$$

where $U_{t,k}$ is the measured voltage at time k.

The online SOC estimation can be completed by substituting Equations (39) and (40) into the above iterative process. The parameters updated online in the FFRLS algorithm will improve the accuracy of the UKF algorithm, including state vector x_k and error covariance P_k. The joint SOC-SOH estimation process of LIBs based on the FFRLS-TLS-UKF algorithm is shown in Figure 4.
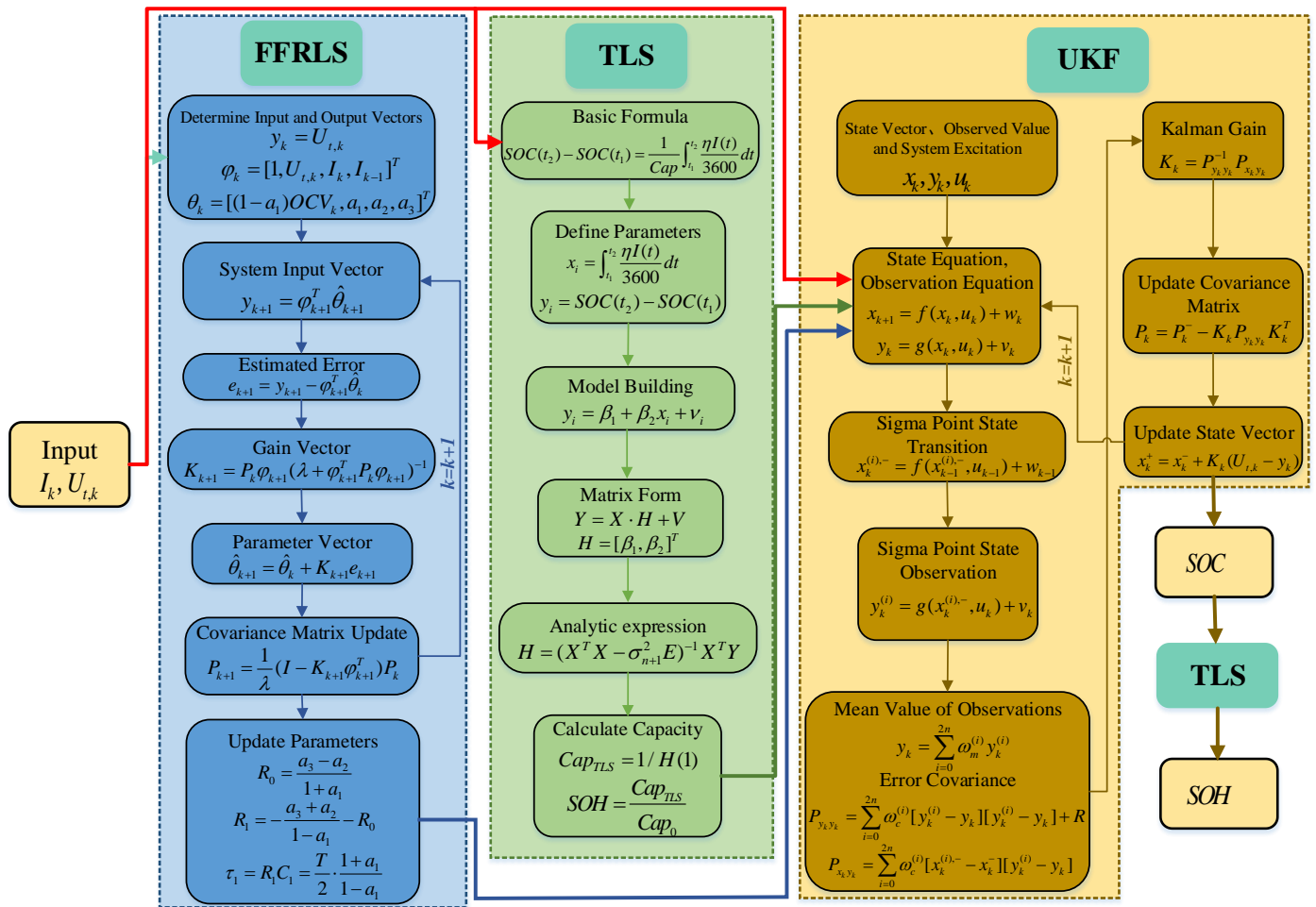
Figure 4. Flow chart of joint SOC-SOH estimation.

4. Experimental Validation

4.1. Experimental Setup

The schematic of the experimental setup is shown in Figure 5. The experimental device is composed of a high-precision battery test system (CT-4008-5V12A-DB), an upper computer, a temperature chamber (BTH-150C), and the 18650 cylindrical battery. The battery test system is connected to the battery in the incubator to control the charging/discharging current and collect data. The upper computer can input commands to control other experimental equipment and store data. The temperature chamber is used to observe and adjust the test temperature. The performance parameters of the experimental battery are shown in Table 1.
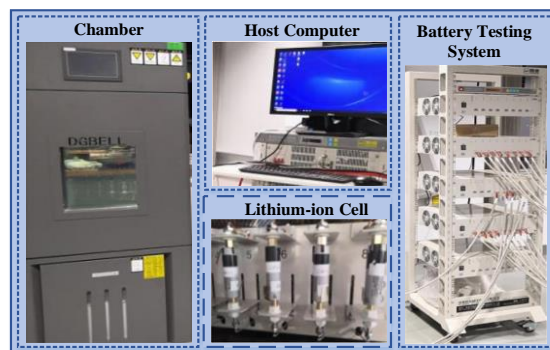

Figure 5. Experimental setup.

Table 1. Battery performance parameters.

Parameters	Values
Positive and negative materials	NCA/C
Capacity (Ah)	3
Nominal voltage (V)	3.6
Charge cutoff voltage (V)	4.2
Discharge cutoff voltage (V)	2.5
Working temperature (°C)	10–45

4.2. Experimental Results

In this paper, the ageing experiments are designed to verify the feasibility of the joint SOC-SOH estimation method based on the FFRLS-TLS-UKF algorithm. The steps of the ageing experiment are shown in Figure 6. The temperature chamber was adjusted to 45 °C, 25 °C, and 10 °C, respectively. Then, the battery was charged at a constant current to SOC = 100% and SOC = 80% at each temperature. Third, the battery was discharged with a constant current of 1/2C to SOC = 0% and SOC = 30%. Fourth, the above process was repeated twice at each temperature and the temperature was adjusted to 25 °C for the basic performance test after completing the cycle, including the standard capacity test, the HPPC test, and the New European Driving Cycle (NEDC) test. The above process is defined as an ageing cycle. The frequency of data acquisition in this paper is 1Hz. The current in an NEDC test is shown in Figure 7.

4.2.1. Results of Parameter Identification

In this study, we first use the PSO algorithm to identify the parameters of the fresh battery at 25 °C to obtain an initial value. The whole SOC region is divided into 10 subregions. In each subregion, the PSO algorithm is used to identify the model parameters offline. Therefore, 10 groups of model parameters are obtained. FFRLS algorithm is then utilized to acquire the model parameters of the target battery online. The results of parameter identification after the first ageing cycle are shown in Figure 8. We can see that the model accuracy is very high (RMSEs of four parameters are 15 mV, 8 mΩ, 16 mΩ and 15 ms, respectively), and the identification value is consistent with the reference value. In addition, the model error in the low SOC region (SOC < 20%) is slightly larger, which is the deficiency of the integer order ECMs.

To better illustrate the effectiveness of the proposed identification, we compare the error between the model's and the measured battery terminal voltage over the full SOC range. Here, six groups of NEDC test data of LIBs with different ageing degrees (SOH down to 86.9%) are selected. The error of terminal voltage between real-time updating and non-updating parameters is shown in Figure 9, with RMSE given in Table 2.

The blue lines in Figure 9 denote the modeling error of using the fresh battery's parameter, and the red line marks the error corresponding to the parameter-adaptive models. As shown in Figure 9, the error of terminal voltage after parameter updating is significantly reduced by 81%, implying an improved modeling accuracy.

Table 2 lists the RMSE of terminal voltage in the whole SOC range before and after parameter updating. When model mismatch does not exist, the parameter-fixed RC model could also achieve a relatively low error (approximately 10 mV). However, this error increases with ageing, especially when SOH < 90%. After using FFRLS to update the model parameters, RMSE drops to 20 mV, which is satisfactory for general engineering use.
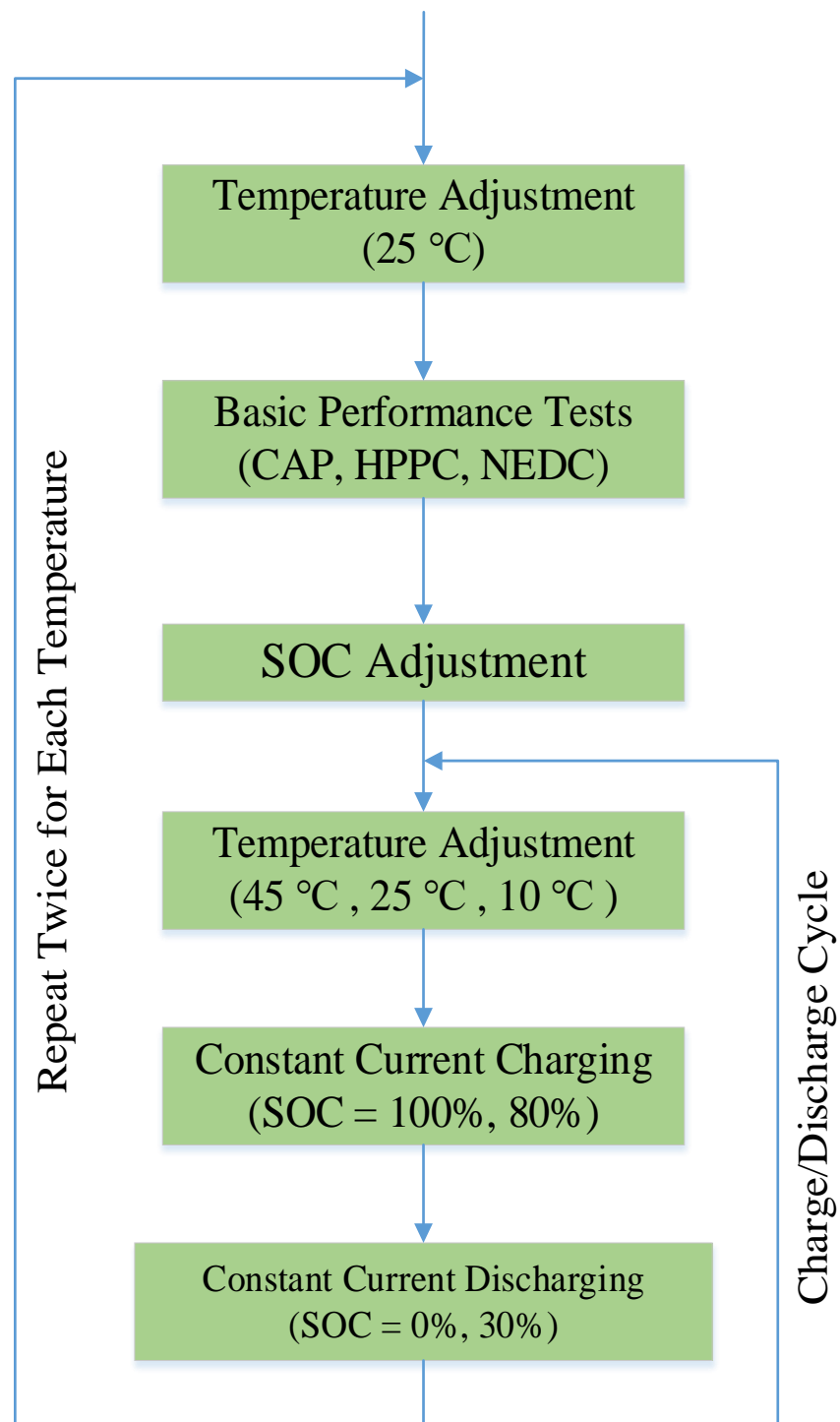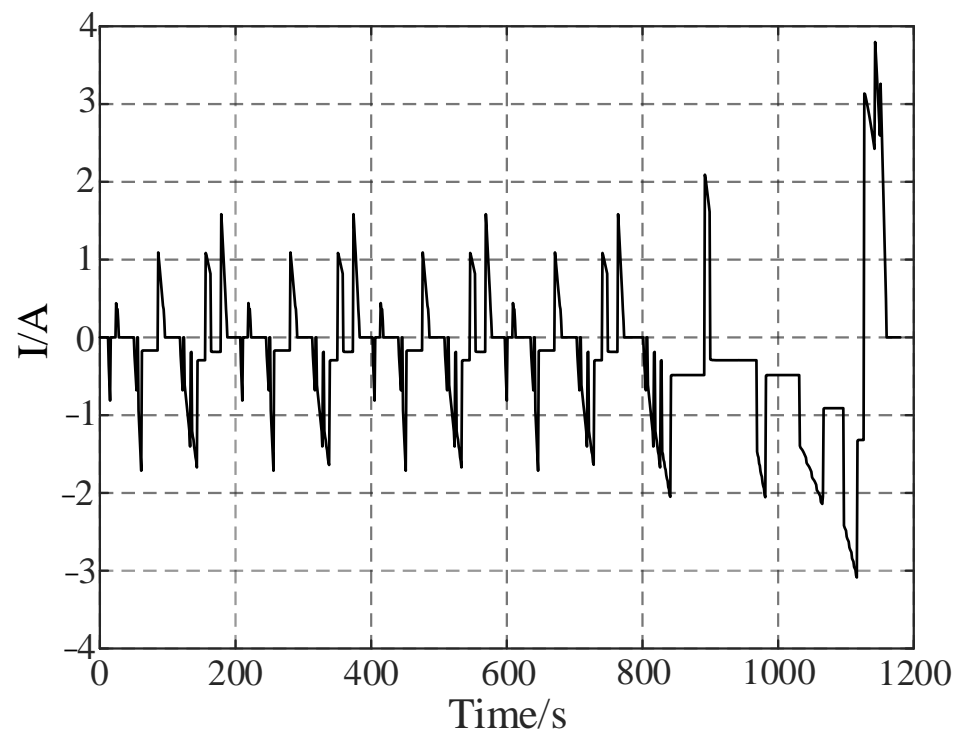
Figure 6. Steps of Ageing Experiment.
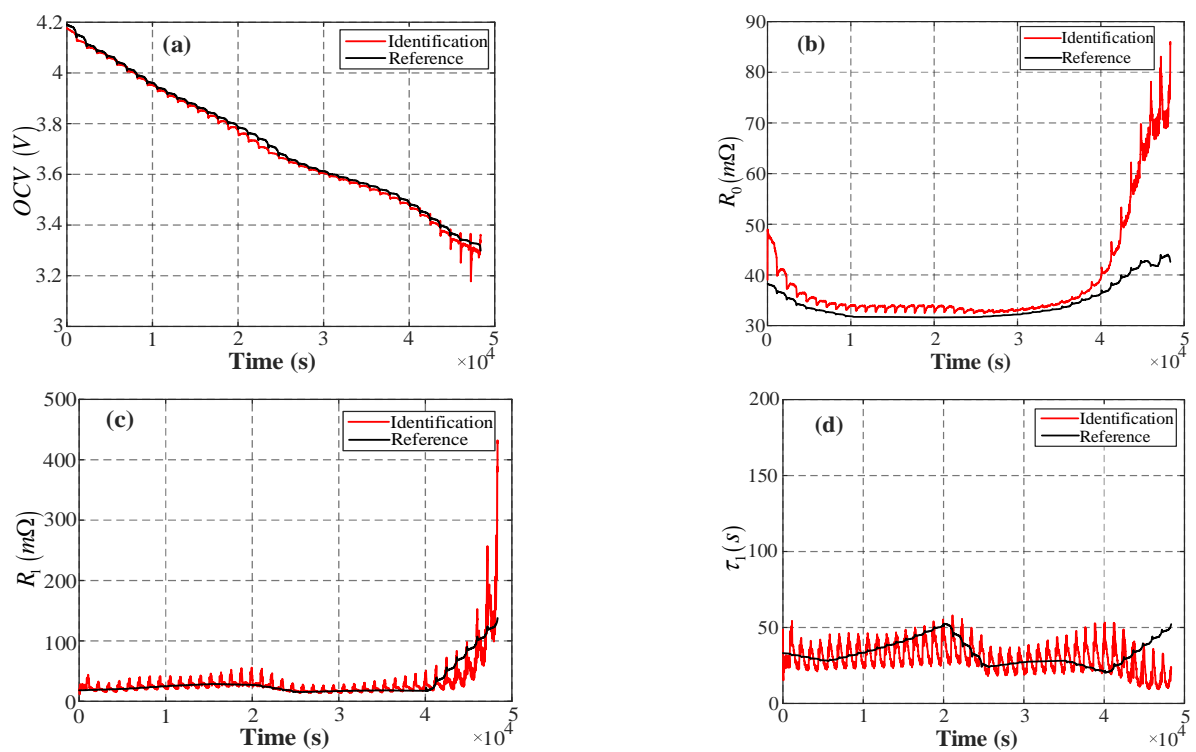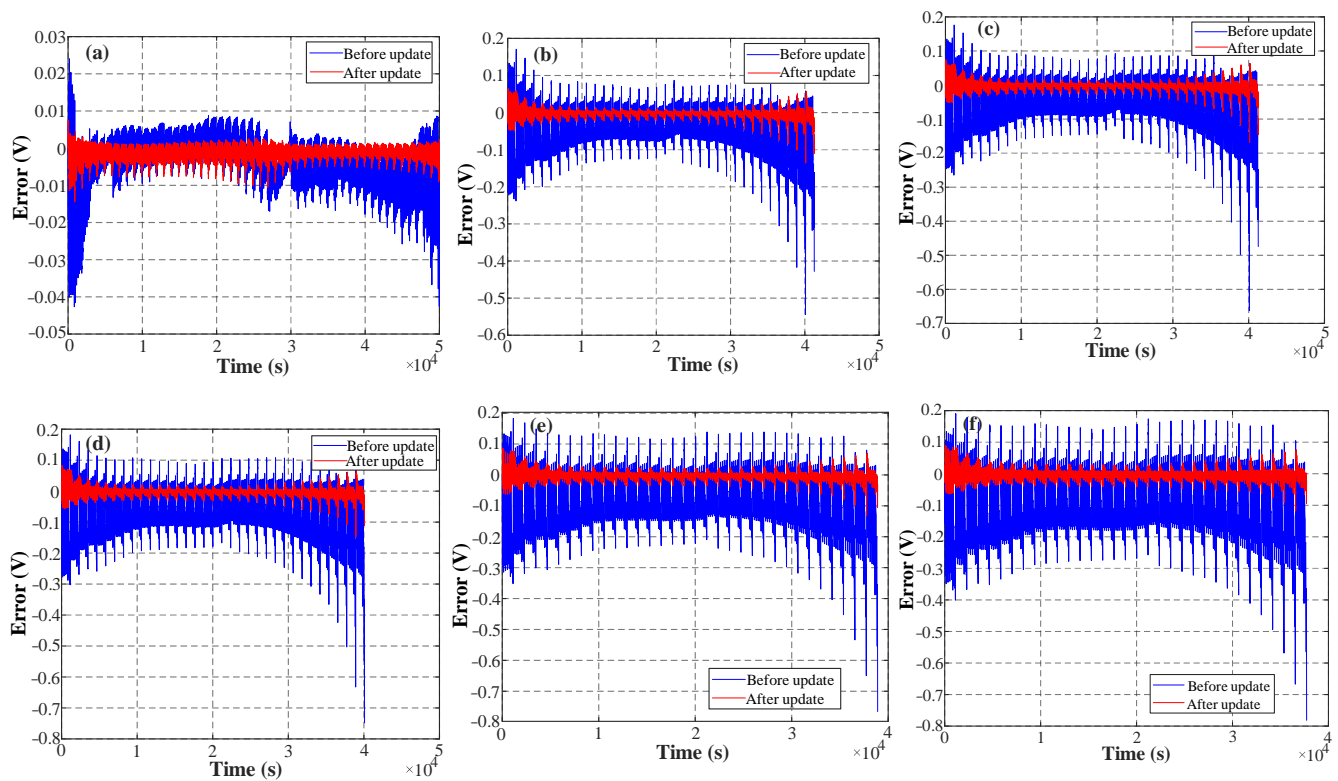
Figure 7. Current in NEDC.

Figure 8. Results of parameter identification after the first ageing cycle: (**a**) OCV, (**b**) R_0, (**c**) R_1, and (**d**) τ_1.

Figure 9. Terminal voltage error under different ageing degrees: (**a**) SOH = 96.2%, (**b**) SOH = 90.2%, (**c**) SOH = 89.8%, (**d**) SOH = 89.2%, (**e**) SOH = 88.3%, and (**f**) SOH = 86.9%.

Table 2. Model errors of batteries with different ageing degrees.

SOH (%)	RMSE (mV) (Before Updating)	RMSE (mV) (After Updating)
100	10.2507	7.6588
96.2	16.2795	9.4335
90.2	63.7639	10.9586
89.8	74.7514	12.5548
89.2	89.1580	13.2999
88.3	105.8686	14.3224
86.9	121.8357	16.0252

4.2.2. Results of SOC Estimation

To verify the effectiveness of the proposed FFRLS-TLS-UKF algorithm in SOC estimation, we use six groups of NEDC test data with different ageing degrees (SOH = 96.2%, 90.2%, 89.8%, 89.2%, 88.3%, and 86.9%) for online parameter identification. The TLS algorithm is used to estimate SOH (in the first stage) to improve the accuracy of prior estimation in the UKF algorithm. Then, SOC is estimated by the UKF algorithm. SOC estimation results under different ageing degrees are shown in Figure 10. The mean absolute error (MAE) and RMSE of SOC estimation are shown in Table 3. The blue line in Figure 10 denotes the SOC reference value obtained by the accurate current integration in our lab, which can be regarded as the referenced value; the green line denotes the SOC estimation results based on the FFRLS-TLS-UKF algorithm; and the red line denotes the SOC estimation results obtained by the UKF algorithm without considering parameter updating. To test the convergence speed of the proposed algorithm, we manually added an initial error of 5% in SOC estimation, and the current and voltage errors are set to $\pm0.001A/V$.

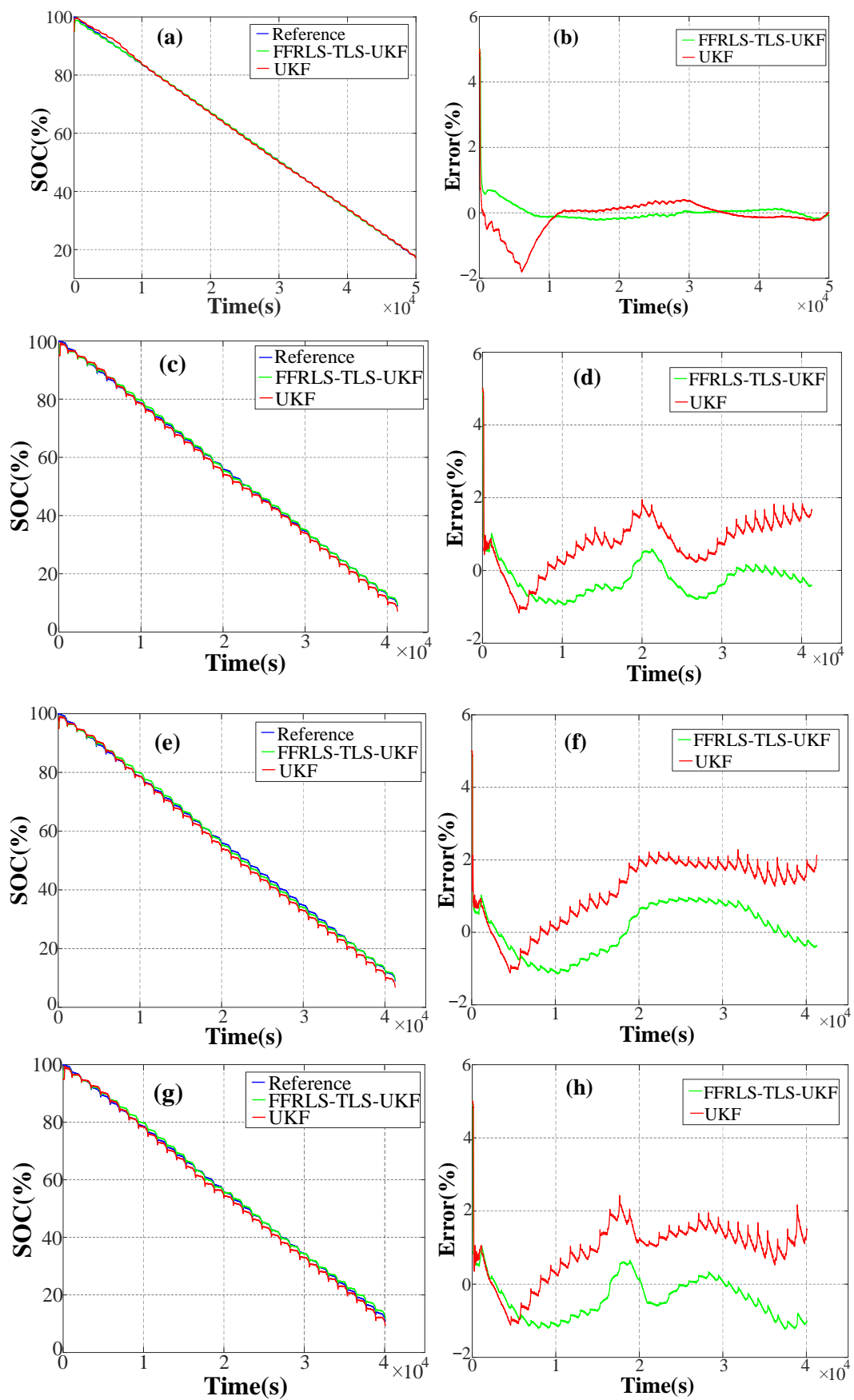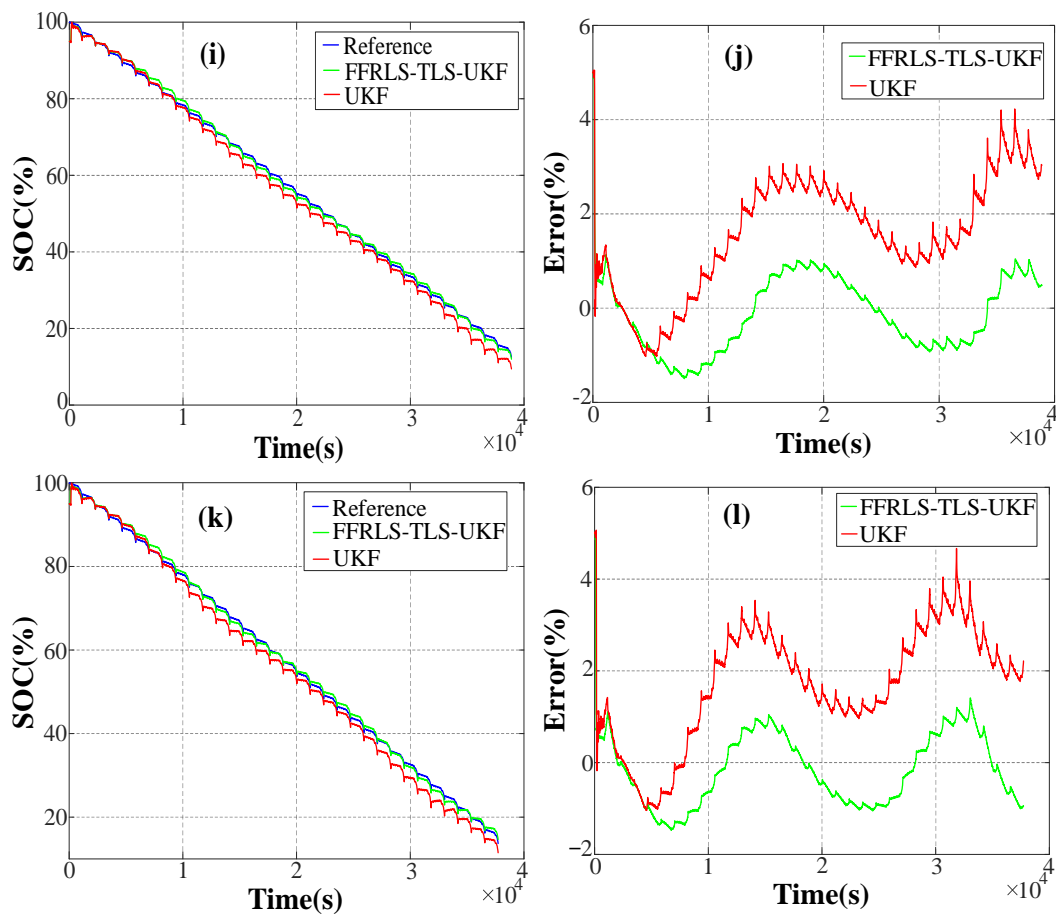**Figure 10.** *Cont.*

Figure 10. Results and errors of SOC estimation under different ageing degrees: (**a**,**b**) SOH = 96.2%; (**c**,**d**) SOH = 90.2%; (**e**,**f**) SOH = 89.8%; (**g**,**h**) SOH = 89.2%; (**i**,**j**) SOH = 88.3%; (**k**,**l**) SOH = 86.9%.

Table 3. MAE and RMSE of SOC estimation.

SOH (%)	MAE (%) (Before Updating)	MAE (%) (After Updating)	RMSE (%) (Before Updating)	RMSE (%) (After Updating)
96.2	0.31	0.16	0.53	0.37
90.2	0.88	0.44	1.02	0.56
89.8	1.27	0.63	1.44	0.73
89.2	1.07	0.58	1.20	0.73
88.3	1.70	0.70	1.97	0.82
86.9	1.84	0.70	2.10	0.81

It can be clearly seen that the SOC estimation using the FFRLS-TLS-UKF algorithm can converge quickly to 2% with the help of real-time updating of model parameters and SOH, even if the capacity difference between the modeling and target batteries exceeds 10% (ranges from 100% to 86.9%). On the contrary, the SOC estimation error without considering parameter updating gradually increases to 4%. It can be concluded that the proposed joint estimation scheme can greatly improve SOC estimation accuracy during battery ageing by at least 50%.

4.2.3. Results of SOH Estimation

After the online model parameter identification, the first-stage SOH (denoted as SOH1 in the following discussions) is estimated by the TLS algorithm. Then, SOH1 is used in SOC estimation to improve accuracy. After SOC estimation, the second-stage SOH (denoted as SOH2 in the following discussions) can be obtained by feeding the estimated

SOC trajectories into the TLS algorithm. For comparison, a benchmarking algorithm that calculates the SOH from the UKF-based SOC trajectory (without parameter update) is also tested, whose result is denoted as SOH3. The SOH estimation results during the battery ageing process and their errors are shown in Figure 11, with RMSE listed in Table 4.
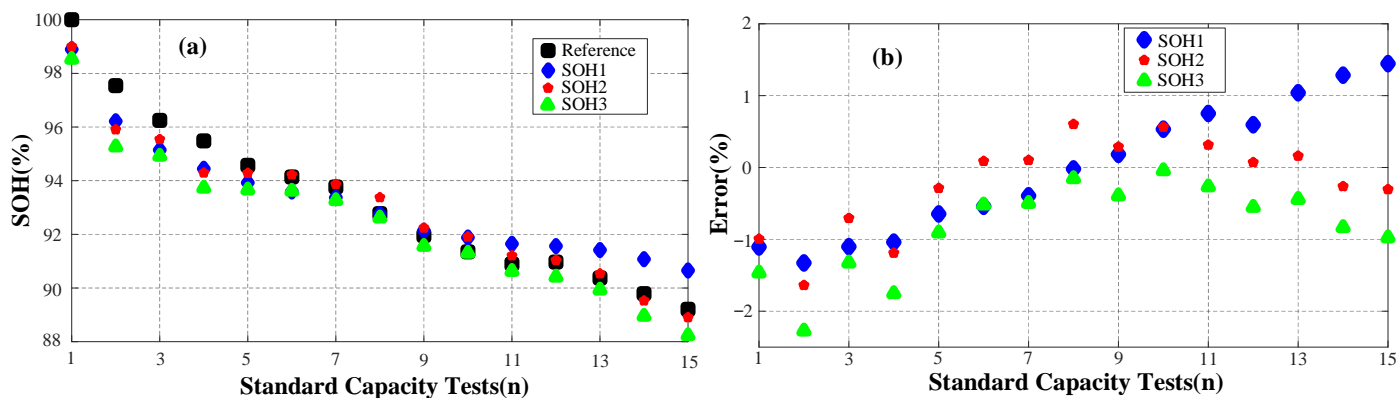

Figure 11. SOH estimation: (**a**) Results, and (**b**) Errors.

Table 4. RMSE of SOH estimation.

Value	RMSE (%)
SOH1	0.90
SOH2	0.67
SOH3	1.03

By comparing SOH2 and SOH3, it is straightforward to see that the SOC accuracy could directly influence the performance of the "Two-Point" SOH estimator. The SOC obtained from the conventional UKF approach suffers from a large chattering issue for aged batteries, and the resulted SOH error becomes large, exceeding 2%. When comparing SOH1 and SOH2, we can see that the second-stage SOH updating is effective. This result agrees with the fact that the FFRLS-UKF algorithm with TLS-updated SOH can provide better SOC estimation accuracy than feeding the online identified OCV into the OCV-SOC lookup table. When comparing SOH1 and SOH3, it is interesting to note that using a powerful UKF algorithm to handle parameter-fixed models is less effective than using a simple FFRLS algorithm to update the parameter-fixed model. This result highlights the importance of adaptive parameter updating in the field of battery management. In addition, the first-stage estimator (SOH1) can also be used independently as an efficient, lightweight SOH observer to save computation.

5. Conclusions

An accurate SOC estimation is key to reducing range anxiety, but it is commonly influenced by the inevitable battery ageing, noting that the battery parameters change gradually with degradation. Here, a joint SOC-SOH estimation method for LIBs based on the FFRLS-TLS-UKF algorithm is proposed to tackle this bottleneck issue, and the following conclusions are drawn:

(1) The FFRLS algorithm is proposed to identify the parameters online. The experimental results indicate that the error of terminal voltage decreases after parameter updating, bounded by 20 mV, even if >10% model mismatch in battery ageing exists;

(2) A two-stage SOH estimator based on the TLS algorithm is proposed, and its error is lower than 2%, exhibiting first-class accuracy. The first-stage SOH estimator can also be used independently to reduce algorithm complexity;

(3) The FFRLS-TLS-UKF algorithm proposed in this paper can effectively improve the accuracy of SOC estimation. The SOC accuracy estimated by the proposed algorithm is

almost twice that estimated by the traditional EKF algorithm. The error is kept within 2% even if there are initial SOC errors, modeling mismatches, and measurement noises.

References

1. Wang, X.; Wei, X.; Zhu, J.; Dai, H.; Zheng, Y.; Xu, X.; Chen, Q. A review of modeling, acquisition, and application of lithium-ion battery impedance for onboard battery management. *eTransportation* **2020**, *7*, 100093. [CrossRef]
2. Song, Z.; Yang, X.-G.; Yang, N.; Delgado, F.P.; Hofmann, H.; Sun, J. A study of cell-to-cell variation of capacity in parallel-connected lithium-ion battery cells. *eTransportation* **2021**, *7*, 100091. [CrossRef]
3. Hao, X.; Yuan, Y.B.; Wang, H.W.; Ouyang, M.G. Plug-in hybrid electric vehicle utility factor in China cities: Influencing factors, empirical research, and energy and environmental application. *eTransportation* **2021**, *10*, 100138. [CrossRef]
4. Hu, G.; Huang, P.; Bai, Z.; Wang, Q.; Qi, K. Comprehensively analysis the failure evolution and safety evaluation of automotive lithium ion battery. *eTransportation* **2021**, *10*, 100140. [CrossRef]
5. Su, L.; Wu, M.; Li, Z.; Zhang, J. Cycle life prediction of lithium-ion batteries based on data-driven methods. *eTransportation* **2021**, *10*, 100137. [CrossRef]
6. Zheng, Y.; Lu, Y.; Gao, W.; Han, X.; Feng, X.; Ouyang, M. Micro-Short-Circuit Cell Fault Identification Method for Lithium-Ion Battery Packs Based on Mutual Information. *IEEE Trans. Ind. Electron.* **2021**, *68*, 4373–4381. [CrossRef]
7. Lai, X.; Chen, Q.; Tang, X.; Zhou, Y.; Gao, F.; Guo, Y.; Bhagat, R.; Zheng, Y. Critical review of life cycle assessment of lithium-ion batteries for electric vehicles: A lifespan perspective. *eTransportation* **2022**, *12*, 100169. [CrossRef]
8. Chen, Q.; Lai, X.; Gu, H.; Tang, X.; Gao, F.; Han, X.; Zheng, Y. Investigating carbon footprint and carbon reduction potential using a cradle-to-cradle LCA approach on lithium-ion batteries for electric vehicles in China. *J. Clean. Prod.* **2022**, *369*, 133342. [CrossRef]
9. Sun, P.; Zhang, H.; Jiang, F.-C.; He, Z.-Z. Self-driven liquid metal cooling connector for direct current high power charging to electric vehicle. *eTransportation* **2021**, *10*, 100132. [CrossRef]
10. Liu, J.; Wang, Z.; Hou, Y.; Qu, C.; Hong, J.; Lin, N. Data-driven energy management and velocity prediction for four-wheel-independent-driving electric vehicles. *eTransportation* **2021**, *9*, 100119. [CrossRef]
11. Wildfeuer, L.; Lienkamp, M. Quantifiability of inherent cell-to-cell variations of commercial lithium-ion batteries. *eTransportation* **2021**, *9*, 100129. [CrossRef]
12. Tang, X.; Liu, K.; Wang, X.; Gao, F.; Macro, J.; Widanage, W.D. Model Migration Neural Network for Predicting Battery Aging Trajectories. *IEEE Trans. Transp. Electrif.* **2020**, *6*, 363–374. [CrossRef]
13. Tang, X.; Wang, Y.; Chen, Z. A method for state-of-charge estimation of LiFePO4 batteries based on a dual-circuit state observer. *J. Power Sources* **2015**, *296*, 23–29. [CrossRef]
14. Lai, X.; He, L.; Wang, S.; Zhou, L.; Zhang, Y.; Sun, T.; Zheng, Y. Co-estimation of state of charge and state of power for lithium-ion batteries based on fractional variable-order model. *J. Clean. Prod.* **2020**, *255*, 120203. [CrossRef]
15. Hu, X.; Feng, F.; Liu, K.; Zhang, L.; Xie, J.; Liu, B. State estimation for advanced battery management: Key challenges and future trends. *Renew. Sustain. Energy Rev.* **2019**, *114*, 109334. [CrossRef]
16. Lai, X.; Huang, Y.; Gu, H.; Han, X.; Feng, X.; Dai, H.; Zheng, Y.; Ouyang, M. Remaining discharge energy estimation for lithium-ion batteries based on future load prediction considering temperature and ageing effects. *Energy* **2021**, *238*, 121754. [CrossRef]
17. Qin, P.; Sun, J.; Yang, X.; Wang, Q. Battery thermal management system based on the forced-air convection: A review. *eTransportation* **2021**, *7*, 100097. [CrossRef]
18. Zhu, S.; Han, J.; An, H.-Y.; Pan, T.-S.; Wei, Y.-M.; Song, W.-L.; Chen, H.-S.; Fang, D. A novel embedded method for in-situ measuring internal multi-point temperatures of lithium ion batteries. *J. Power Sources* **2020**, *456*, 227981. [CrossRef]
19. Xiong, R.; Yu, Q.; Wang, L.Y.; Lin, C. A novel method to obtain the open circuit voltage for the state of charge of lithium ion batteries in electric vehicles by using H infinity filter. *Appl. Energy* **2017**, *207*, 346–353. [CrossRef]
20. Xiong, R.; Cao, J.; Yu, Q.; He, H.; Sun, F. Critical Review on the Battery State of Charge Estimation Methods for Electric Vehicles. *IEEE Access* **2018**, *6*, 1832–1843. [CrossRef]

21. Han, X.; Ouyang, M.; Lu, L.; Li, J.; Zheng, Y.; Li, Z. A comparative study of commercial lithium ion battery cycle life in electrical vehicle: Aging mechanism identification. *J. Power Sources* **2014**, *251*, 38–54. [CrossRef]

22. Yin, H.; Ma, S.; Li, H.; Wen, G.; Santhanagopalan, S.; Zhang, C. Modeling strategy for progressive failure prediction in lithium-ion batteries under mechanical abuse. *eTransportation* **2021**, *7*, 100098. [CrossRef]

23. Deshpande, R.D.; Bernardi, D.M. Modeling Solid-Electrolyte Interphase (SEI) Fracture: Coupled Mechanical/Chemical Degradation of the Lithium Ion Battery. *J. Electrochem. Soc.* **2017**, *164*, A461–A474. [CrossRef]

24. Wu, B.; Lu, W. Mechanical Modeling of Particles with Active Core–Shell Structures for Lithium-Ion Battery Electrodes. *J. Phys. Chem. C* **2017**, *121*, 19022–19030. [CrossRef]

25. Ali, Y.; Lee, S. An integrated experimental and modeling study of the effect of solid electrolyte interphase formation and Cu dissolution on $CuCo_2O_4$-based Li-ion batteries. *Int. J. Energy Res.* **2022**, *46*, 3017–3033. [CrossRef]

26. Laue, V.; Röder, F.; Krewer, U. Practical identifiability of electrochemical P2D models for lithium-ion batteries. *J. Appl. Electrochem.* **2021**, *51*, 1253–1265. [CrossRef]

27. Cui, Z.; Wang, L.; Li, Q.; Wang, K. A comprehensive review on the state of charge estimation for lithium-ion battery based on neural network. *Int. J. Energy Res.* **2022**, *46*, 5423–5440. [CrossRef]

28. Shu, X.; Li, G.; Shen, J.; Lei, Z.; Chen, Z.; Liu, Y. A uniform estimation framework for state of health of lithium-ion batteries considering feature extraction and parameters optimization. *Energy* **2020**, *204*, 117957. [CrossRef]

29. Che, Y.; Deng, Z.; Tang, X.; Lin, X.; Nie, X.; Hu, X. Lifetime and Aging Degradation Prognostics for Lithium-ion Battery Packs Based on a Cell to Pack Method. *Chin. J. Mech. Eng.* **2022**, *35*, 4. [CrossRef]

30. Li, S.; He, H.; Li, J. Big data driven lithium-ion battery modeling method based on SDAE-ELM algorithm and data pre-processing technology. *Appl. Energy* **2019**, *242*, 1259–1273. [CrossRef]

31. Shu, X.; Shen, S.; Shen, J.; Zhang, Y.; Li, G.; Chen, Z.; Liu, Y. State of health prediction of lithium-ion batteries based on machine learning: Advances and perspectives. *iScience* **2021**, *24*, 103265. [CrossRef] [PubMed]

32. Lai, X.; Qiao, D.; Zheng, Y.; Zhou, L. A Fuzzy State-of-Charge Estimation Algorithm Combining Ampere-Hour and an Extended Kalman Filter for Li-Ion Batteries Based on Multi-Model Global Identification. *Appl. Sci.* **2018**, *8*, 2028. [CrossRef]

33. Ling, L.; Sun, D.; Yu, X.; Huang, R. State of charge estimation of Lithium-ion batteries based on the probabilistic fusion of two kinds of cubature Kalman filters. *J. Energy Storage* **2021**, *43*, 103070. [CrossRef]

34. Lai, X.; Yi, W.; Cui, Y.; Qin, C.; Han, X.; Sun, T.; Zhou, L.; Zheng, Y. Capacity estimation of lithium-ion cells by combining model-based and data-driven methods based on a sequential extended Kalman filter. *Energy* **2020**, *216*, 119233. [CrossRef]

35. Tang, X.; Wang, Y.; Zou, C.; Yao, K.; Xia, Y.; Gao, F. A novel framework for Lithium-ion battery modeling considering uncertainties of temperature and aging. *Energy Convers. Manag.* **2018**, *180*, 162–170. [CrossRef]

36. Boulmrharj, S.; Ouladsine, R.; NaitMalek, Y.; Bakhouya, M.; Zine-Dine, K.; Khaidar, M.; Siniti, M. Online battery state-of-charge estimation methods in micro-grid systems. *J. Energy Storage* **2020**, *30*, 101518. [CrossRef]

37. Yang, X.; Chen, Y.; Li, B.; Luo, D. Battery states online estimation based on exponential decay particle swarm optimization and proportional-integral observer with a hybrid battery model. *Energy* **2020**, *191*, 116509. [CrossRef]

38. Zheng, W.; Xia, B.; Wang, W.; Lai, Y.; Wang, M.; Wang, H. State of Charge Estimation for Power Lithium-Ion Battery Using a Fuzzy Logic Sliding Mode Observer. *Energies* **2019**, *12*, 2491. [CrossRef]

39. Zhang, J.; Wang, P.; Gong, Q.; Cheng, Z. SOH estimation of lithium-ion batteries based on least squares support vector machine error compensation model. *J. Power Electron.* **2021**, *21*, 1712–1723. [CrossRef]

40. Yu, Q.; Xiong, R.; Yang, R.; Pecht, M.G. Online capacity estimation for lithium-ion batteries through joint estimation method. *Appl. Energy* **2019**, *255*, 113817. [CrossRef]

41. Tan, X.; Zhan, D.; Lyu, P.; Rao, J.; Fan, Y. Online state-of-health estimation of lithium-ion battery based on dynamic parameter identification at multi timescale and support vector regression. *J. Power Sources* **2021**, *484*, 229233. [CrossRef]

42. Yan, W.; Zhang, B.; Zhao, G.; Tang, S.; Niu, G.; Wang, X. A Battery Management System With a Lebesgue-Sampling-Based Extended Kalman Filter. *IEEE Trans. Ind. Electron.* **2019**, *66*, 3227–3236. [CrossRef]

43. Tang, X.; Gao, F.; Liu, K.; Liu, Q.; Foley, A.M. A Balancing Current Ratio Based State-of-Health Estimation Solution for Lithium-Ion Battery Pack. *IEEE Trans. Ind. Electron.* **2022**, *69*, 8055–8065. [CrossRef]

44. Hu, X.; Li, S.; Peng, H. A comparative study of equivalent circuit models for Li-ion batteries. *J. Power Sources* **2012**, *198*, 359–367. [CrossRef]

45. Lai, X.; Qin, C.; Gao, W.; Zheng, Y.; Yi, W. A State of Charge Estimator Based Extended Kalman Filter Using an Electrochemistry-Based Equivalent Circuit Model for Lithium-Ion Batteries. *Appl. Sci.* **2018**, *8*, 1592. [CrossRef]

46. Lai, X.; Zheng, Y.; Sun, T. A comparative study of different equivalent circuit models for estimating state-of-charge of lithium-ion batteries. *Electrochim. Acta* **2018**, *259*, 566–577. [CrossRef]

47. Wei, Z.; Zou, C.; Leng, F.; Soong, B.H.; Tseng, K.-J. Online Model Identification and State-of-Charge Estimate for Lithium-Ion Battery With a Recursive Total Least Squares-Based Observer. *IEEE Trans. Ind. Electron.* **2017**, *65*, 1336–1346. [CrossRef]

48. Lai, X.; Gao, W.; Zheng, Y.; Ouyang, M.; Li, J.; Han, X.; Zhou, L. A comparative study of global optimization methods for parameter identification of different equivalent circuit models for Li-ion batteries. *Electrochim. Acta* **2018**, *295*, 1057–1066. [CrossRef]

49. Sun, X.; Ji, J.; Ren, B.; Xie, C.; Yan, D. Adaptive Forgetting Factor Recursive Least Square Algorithm for Online Identification of Equivalent Circuit Model Parameters of a Lithium-Ion Battery. *Energies* **2019**, *12*, 2242. [CrossRef]

50. Sun, C.; Lin, H.; Cai, H.; Gao, M.; Zhu, C.; He, Z. Improved parameter identification and state-of-charge estimation for lithium-ion battery with fixed memory recursive least squares and sigma-point Kalman filter. *Electrochim. Acta* **2021**, *387*, 138501. [CrossRef]
51. Tang, X.; Zou, C.; Yao, K.; Chen, G.; Liu, B.; He, Z.; Gao, F. A fast estimation algorithm for lithium-ion battery state of health. *J. Power Sources* **2018**, *396*, 453–458. [CrossRef]
52. Zheng, Y.; Cui, Y.; Han, X.; Dai, H.; Ouyang, M. Lithium-ion battery capacity estimation based on open circuit voltage identification using the iteratively reweighted least squares at different aging levels. *J. Energy Storage* **2021**, *44*, 103487. [CrossRef]
53. Tang, X.; Liu, K.; Liu, Q.; Peng, Q.; Gao, F. Comprehensive study and improvement of experimental methods for obtaining referenced battery state-of-power. *J. Power Sources* **2021**, *512*, 230462. [CrossRef]
54. Markovsky, I.; Van Huffel, S. Overview of total least-squares methods. *Signal Process.* **2007**, *87*, 2283–2302. [CrossRef]
55. Yu, Q.; Wan, C.; Li, J.; E, L.; Zhang, X.; Huang, Y.; Liu, T. An Open Circuit Voltage Model Fusion Method for State of Charge Estimation of Lithium-Ion Batteries. *Energies* **2021**, *14*, 1797. [CrossRef]
56. Lai, X.; Yi, W.; Zheng, Y.; Zhou, L. An All-Region State-of-Charge Estimator Based on Global Particle Swarm Optimization and Improved Extended Kalman Filter for Lithium-Ion Batteries. *Electronics* **2018**, *7*, 321. [CrossRef]
57. Lin, X.; Tang, Y.; Ren, J.; Wei, Y. State of charge estimation with the adaptive unscented Kalman filter based on an accurate equivalent circuit model. *J. Energy Storage* **2021**, *41*, 102840. [CrossRef]
58. He, Z.; Li, Y.; Sun, Y.; Zhao, S.; Lin, C.; Pan, C.; Wang, L. State-of-charge estimation of lithium ion batteries based on adaptive iterative extended Kalman filter. *J. Energy Storage* **2021**, *39*, 102593. [CrossRef]